

EVOLUTION OF THE 3D MICROSTRUCTURE OF A SHORT FIBRE REINFORCED AL-SI ALLOY DURING CREEP

Guillermo C. Requena*, Hans P. Degischer*, Esteban D. Marks*, Elodie Boller**

*Vienna Univ. of Technology - Austria, **European Synchrotron Radiation Facility - France

Keywords: *micro-tomography, short fibre reinforced metals, creep, hybrid reinforcement, Si coarsening, void formation.*

Abstract

The evolution of the microstructure during creep of an AlSi12CuMgNi alloy with 15 vol% of Al₂O₃ short fibres is investigated by means of synchrotron micro-tomography. The results reveal a change of the morphology of the hybrid reinforcement composed by the eutectic-Si, the short fibres and the intermetallic particles. This change takes place due to the diffusion induced spheroidisation and coarsening of Si and of the intermetallic particles. The interconnectivity of the hybrid reinforcement increases during long-term creep exposure reaching almost full connectivity after 6400 h of creep.

The analysis of creep damage during secondary creep stage shows the increase of the void volume fraction by a factor of 2, while the number of voids per volume remains practically constant. An analysis of the voids' location indicates that pores generated during the processing of the composite grow and no new pores are produced during the primary and secondary creep stage.

1 Introduction

Short fibre reinforced metals (SFRMs) [1] are directly strengthened by means of an effective transfer of the applied load from the matrix to the short fibres (SFs) [2] which is increasingly effective at elevated temperatures. In creep conditions, this transfer of load results in a redistribution of internal stresses within the sample, which provokes a reduction of the driving force for matrix creep and therefore a reduction of the creep rate in the matrix [3-4]. The ceramic reinforcement does not creep at the considered condition.

In the case of Al-Si based SFRMs with Si content >7 wt.%, the eutectic Si and the SFs form a three-dimensional hybrid network [5] in which the SFs are connected by Si bridges. The strength and stability of this structure is sensitive to the size and amount of the Si bridges. Furthermore, the morphology of the eutectic Si varies during high temperature exposure due to the diffusion driven spheroidisation [5] resulting in a subsequent change of the interconnectivity of the hybrid Si-SFs structure.

Results of the long-term creep behaviour of an AlSi12CuMgNi-based SFRM produced by squeeze casting tested at 300°C have been reported in [4]. During the creep tests, the SFRMs showed a decrease in stationary strain rate after a period of moderate load increasing (<20% of the yield stress) as well as an increase of the creep exponent n . Such a “training” effect reduces, for example, the stationary creep rate of $3.5 \times 10^{-10} \text{ s}^{-1}$ achieved at 30 MPa for the SFRM by about 50% after a load increase of 10 MPa for about 400 h [4]. It has been proposed [4] that one of the reasons for the creep strengthening of short fibre reinforced Al-Si alloys during long term creep exposure is the Si diffusion induced increase of the interconnectivity of the Si-SF hybrid structure. Hardness tests carried out on the hybrid Si-SF-intermetallics structure showed an increase of the rigidity of this network with increasing creep exposure times [4]. However, no data are available on the real architecture and its evolution during long-term creep for this kind of composites. This information is necessary if the mechanical properties of the composite are to be correlated with the microstructure of the SFRM and the experimental observations.

The creep resistance of SFRMs is affected by the orientation angle β between the reinforcing SFs

and the applied load. Klipfel et al. [6] showed that only those SFs within an angular range between $(-\beta_T; \beta_T)$, where $\beta_T \approx 63^\circ$ effectively reinforce the matrix in tension at RT. At elevated temperatures, the critical fibre length increases so that the angular range for β_T will be decreased significantly. Taking into account that the diffusion of Si causes its spheroidisation in the surrounding of the SFs, the possibility of reorientation of the SFs during long-term creep may occur due to matrix diffusion enhanced by the creep stress. This effect and its consequences on the creep resistance of SFRMs will also be analysed in this work.

On the other hand, light optical and scanning electron microscopy of the untested AlSi12CuMgNi-based SFRMs revealed the presence of pores with a few μm diameter at the interface between adjacent fibres as well as between fibres and eutectic Si or intermetallic inclusions. Damage analysis of crept samples suggested that fracture of fibres starts at about 1% strain independent of the external load [4].

During the present investigations, micro-computed tomography (μCT) was carried out for the same AlSi12CuMgNi-based SFRM as in [4] before and after 6400 h of creep. The objectives were:

- to study the Si-SFs hybrid network to reveal its evolution and the change of interconnectivity during long-term creep exposure.
- to study the reorientation of the reinforcement during long-term creep exposure.
- to study the damage process in SFRMs, focusing on the fracture of the SFs and the determination of the sites of formation and growth of voids both during the fabrication of the composite as well as during long term creep exposure.

2 Experimental

2.1 Description of Materials

The SRFM presented in this work is an AlSi12CuMgNi alloy reinforced with 15vol% of SFs. The matrix alloy is typically used for combustion engines [7]. Its chemical composition can be seen in Table 1. The SFRM was produced at the Institute of Materials Science and Technology at the TU Clausthal in Germany using a squeeze casting process as reported in [8]. Preforms of randomly planar distributed Saffil® SFs consisting of 96-97% Al_2O_3 and 3-4% SiO_2 [9] were used as reinforcement. The SFs have lengths ranging from 10 to 200 μm with diameters between 1 and 10 μm .

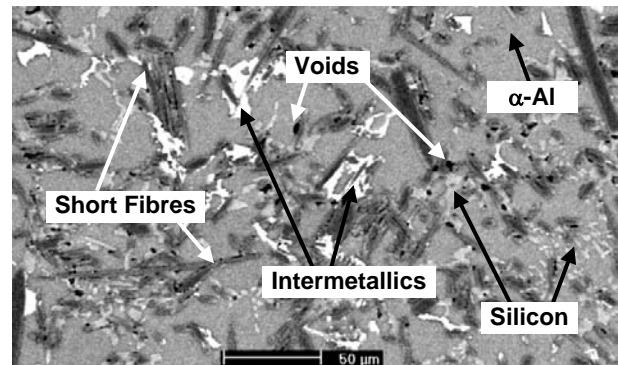


Fig. 1. SEM micrograph showing the constituents of the composite: $\alpha\text{-Al}$ (background), eutectic Si (bright grey), Fe- and Ni-rich intermetallics (white), Al_2O_3 -SFs (dark grey) with pores (black) at the interfaces. The plane shown corresponds to the plane of random planar fibre orientation in which the creep stress acted vertically.

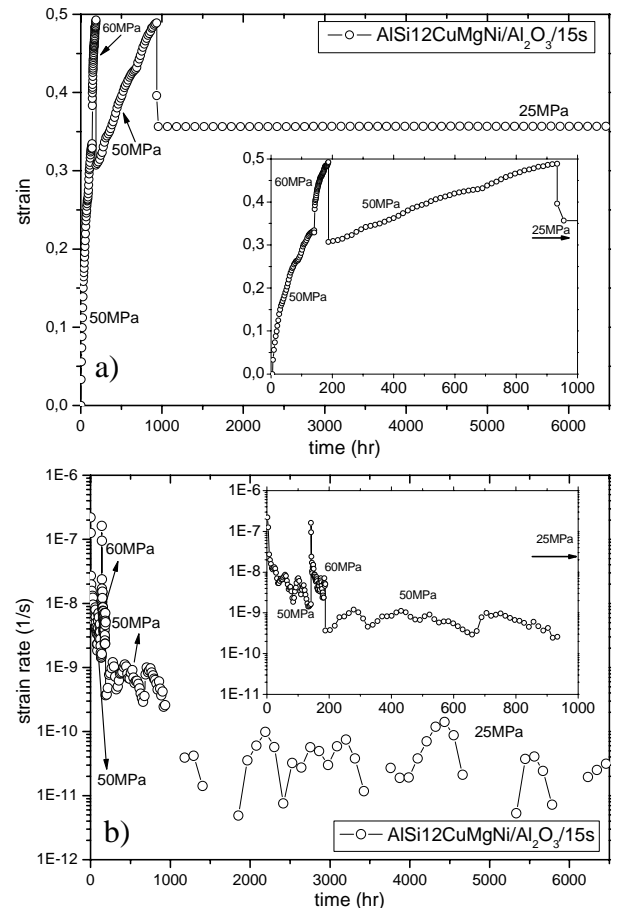


Fig. 2. a) strain vs. t and b) strain rate vs. t curves obtained for the investigated GP condition during creep with changes of load (50 MPa/140 h \rightarrow 60 MPa/50 h \rightarrow 50 MPa/745 h \rightarrow 25 MPa/5465 h). The zoomed region shows the first 1000 h of creep where a reduction of stationary creep rate can be observed at 50 MPa after the period of 60 MPa.

Fig. 1 shows the microstructure of the SFRM in T6S condition looking onto the plane of random orientation. Besides the SFs and the matrix, the eutectic Si (grey), Fe- and Ni-rich intermetallic phases (white) and some pores (black) at the interface between the matrix and SFs and between adjacent fibres are observable. These pores show up during the processing of the composite since the squeeze casting process may not be able to feed all the shrinkage pores during solidification due to the decreased fibres' interspacing [10].

Table 1. Chemical composition of the AlSi12CuMgNi matrix alloy [11].

Element	Si	Cu	Mg	Ni	Fe	Mn	Zn	Ti
wt.%	11-13	0.8-1.3	0.8-1.3	1.3	0.7	0.3	0.3	0.2

The SFRM was investigated in 2 different conditions:

- a) T6S condition: solution treated at 480°C/4h + oil quenched + annealing at 190°C/4h + overaging at 300°C/3h
- b) GP condition after 6400h of creep at 300°C as shown in Fig. 2 by (a) strain vs. time and (b) strain rate vs. time curves. A detailed description of the methodology employed for the creep investigations can be found in [4].

2.2 Micro-tomography

μCT was carried out at the ID19 beamline at the European Synchrotron Radiation (ESRF) in Grenoble [12], France. The energy used was 21.2 keV. The μCT projections were recorded using a 2D CCD camera developed at ESRF using an effective pixel size of 0.7 μm. 800 projections have been recorded. The phase contrast mode [13] was used for the acquisition of the μCT projections. For this, a distance of 20 mm between the camera and the sample was selected. The edge enhancement resulting from the phase contrast mode produces the necessary contrast between phases having similar mass densities, as it is the case for the Al matrix and the Si, present in the investigated SFRM [14]. The reconstructed μCT volume has a final size of 2048x2048x2048 voxels, with a voxel size of (0.7 μm)³.

2.3 Image Analysis

The qualitative and quantitative image analysis of the morphology and interconnectivity of the Si-SFs hybrid network as well as of the type and sites of damage within the reconstructed μCT volumes

was carried out using the ImageJ, Amira and VGStudioMax softwares [15-17]. A minimum size of 8 voxels and 27 voxels was taken for the quantitative analysis of voids and Si, respectively. Since the phase contrast mode was used for the μCT scans, the presence of Fresnel fringes [12] around the SFs can lead to an overestimation of the pore volume fraction. Therefore, only a comparative analysis between the different material conditions can be carried out.

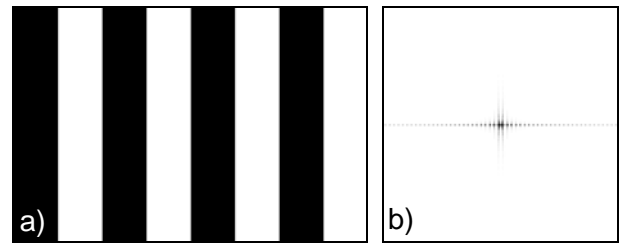


Fig. 3. FFT Transform. a) Original 2D image of vertical stripes and b) transformed into the frequency domain producing a pattern perpendicular to the main orientation direction of the original image.

The 3D Fast Fourier Transform (FFT) algorithm [18] was used to study the change of fibres' orientation during creep exposure. The FFT method, transforms an image from the spatial domain into the frequency domain, where each point represents a particular frequency contained in the original image. The image in the frequency domain will show an alignment of points (particular frequencies) along the directions where the intensity of the image in the spatial domain present intensity changes. Taking this property into account, the orientation of the SFs in the studied composite will be perpendicular to the direction of alignment of periodical frequencies. If a mean preferential orientation of the fibres is present in the composite, this should be detectable in the spectrum obtained after applying the FFT. This is illustrated schematically in the example shown in Fig. 3 for the case of a 2D transformation, where a periodical arrangement of vertical stripes (a) is transformed into the frequency domain (b) using the FFT. The obtained spectrum in the frequency domain shows an alignment of points along the horizontal axis, which is in fact perpendicular to the vertical stripes in the space domain. The 3D FFT works in the same way as the 2D FFT but operates in the 3D space. This means that the pattern of particular frequencies in the transformed image will be a volume with a longer axis (for example the major axis of an ellipsoid) perpendicular to the main orientation direction in the original volume. Binarized

reconstructed volumes of the SFs were used as input data in order to avoid interference with any of the other components of the SFRM. The calculations were carried out using the plug in FFTJ and DeconvolutionJ for ImageJ described in [19]. The sensitivity of the method was tested applying a manual orientation of the SFs and was found to be about 6°.

3 Results

3.1 3D Structure of the SFRM

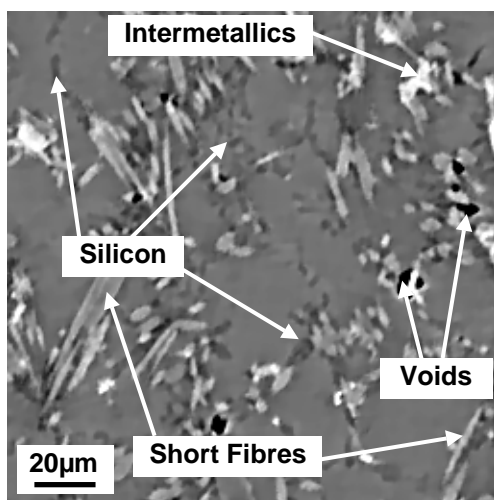


Fig. 4. Reconstructed μ CT slice with a size of 256x256 pixels for the crept GP condition showing the constituents of the SFRM (compare with Fig. 1).

Fig. 4 shows a portion of a reconstructed slice with a size of 256x256 pixels obtained from the μ CT scans for the crept GP condition. The constituents of the composites can be clearly identified by their different grey values. Special care has to be taken for the case of the Si, which can be confused with the matrix if an automatic segmentation is carried out. This requires a much more time-consuming hand segmentation for this phase.

Fig. 5 shows a typical reconstructed volume of the GP sample, where all the constituents of the composite can be observed except the Al matrix, which has been made transparent for better clarity. The size of this volume is 100x100x240 voxels. The yellow phase is the Si, the grey one are the SFs, in red are shown the voids and the particles with other colours are individual intermetallic particles. Fig. 5 a) shows all the components together (SFs, intermetallics, Si and voids). The already mentioned Si-SF hybrid structure can be clearly observed and it is also observable that the intermetallic phases also contribute to build this interconnected network. Fig. 5 b) shows only the Si, c) the SFs, the voids and the intermetallic phases and d) only the voids and the intermetallics.

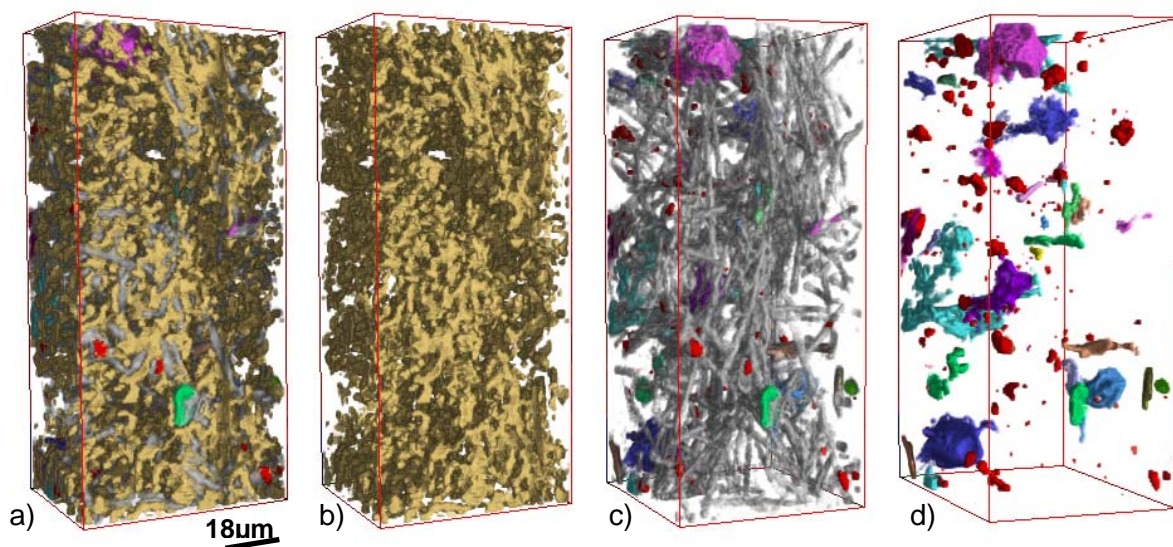


Fig. 5. Reconstructed volume of the crept SFRM (GP condition) showing the Si (yellow), SFs (grey), voids (red) and the intermetallic particles (rest of particles) (a) all together, (b) only the Si, (c) SFs, intermetallic particles and voids and (d) intermetallic particles and voids. Size of the volume: 100x100x240 voxels. The vertical axis corresponds to the load direction.

3.2 Interconnectivity of the Hybrid Structure

Fig. 6 a) and Fig. 7 a) show typical light optical micrographs of the composite in T6S condition and after 6400 h of creep exposure (GP), respectively. The pictures on the right (Fig. 6 b and Fig. 7 b) are binarized images of the same regions as in a) showing only the Si phase. It can be clearly observed by eye that the Si particles are coarser in the GP condition. A quantitative analysis of the size of Si particles for different regions of the composite in both studied conditions shows that the mean Si particle cross section grows from $7.6 \pm 0.8 \mu\text{m}^2$ for T6S to $14.9 \pm 1 \mu\text{m}^2$ for GP. Furthermore, the Si particle density (calculated as the amount of particles per picture area) goes from 184 ± 12 particles/Mpixel for T6S down to 117 ± 24 particles/Mpixel. This 2D analysis clearly shows that the spheroidisation of Si takes also place during sufficiently long creep exposure at a temperature as low as 300°C , where the solubility of Si is only 0.1 at% [20]. However, this analysis gives no information on the actual 3D size of the Si particles and on the possible connections between one or more Si regions.

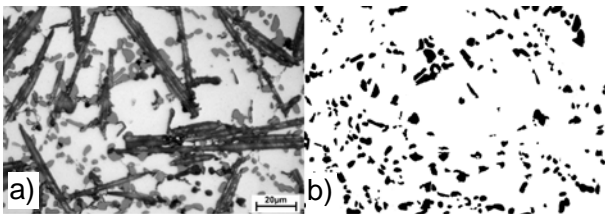


Fig. 6. a) Light optical micrograph of the SFRM in T6S condition. b) Binarized image of the same region as in a) where only the Si is visible. Mean Si particle size: $7.6 \pm 0.8 \mu\text{m}^2$.

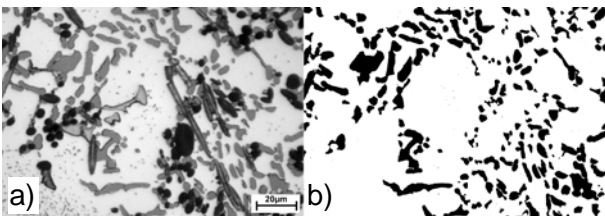


Fig. 7. a) Light optical micrographs of the SFRM after 6400 h of creep exposure (GP condition). b) Binarized image of the same region as in a) where only the Si is visible. Mean Si particle size: $14.9 \pm 1 \mu\text{m}^2$.

The interconnectivity between Si, SFs and intermetallics was studied in volumes of $150 \times 150 \times 150$ voxels for which a minimum particle size of 27 voxels ($\sim 9.3 \mu\text{m}^3$) was considered. The results are shown in Table 2 and

Table 3 for the composite in T6S and GP conditions, respectively. The volume fraction of Si in both conditions is between 7 and 8 vol%, which is smaller than the Si volume fraction of the alloy (12 vol%) but this is due to the small volumes used for the quantitative study. However, this does not affect the obtained results relatively since the differences between both phases are clearly marked. The amount of Si particles in the investigated volumes for T6S condition is about three times larger than after 6400 h of creep exposure. Furthermore, the biggest Si particle for the T6S condition accumulates less than 7 % of the Si content. The results for the GP sample show that the biggest Si particle has grown to accumulate almost 70% of the total Si content. This considerable increase of the connectivity can be seen in Fig. 8 and Fig. 9, where all the Si particles of two of the investigated volumes are depicted in (a) showing the biggest Si particle in (b).

Table 2. Volume fraction of Si, SFs+intermetallics and Si+SFs+intermetallics and relative accumulated volumes of the biggest interconnected structures in T6S condition.

Components	f (vol%)	Biggest Particle (% of f)
Si	7.7 ± 0.4	6.6 ± 3.4
SF+Intermetallics	11.7 ± 1.5	60.7 ± 7.6
Si+SF+Intermetallics	19.4 ± 1.5	95.3 ± 1.4

Table 3. Volume fraction of Si, SFs+intermetallics and Si+SFs+intermetallics and relative accumulated volumes of the biggest interconnected structures in the crept GP condition.

Components	f (vol%)	Biggest Particle (% of f)
Si	6.8 ± 0.5	69.2 ± 3.4
SF+Intermetallics	17.4 ± 2.9	96.6 ± 0.5
Si+SF+Intermetallics	24 ± 2.8	99.2 ± 0.2

A total volume fraction of $11.7 \pm 1.5 \text{ vol}\%$ is obtained for T6S if the SFs are analysed together with the intermetallics. The GP condition shows an increase in volume fraction of SFs+intermetallics of about 30% ($17.4 \pm 2.9 \text{ vol}\%$), which may be related to a coarsening of the intermetallic particles, indicating that about 5 vol% of the intermetallics are below the chosen threshold of 27 voxels in the T6S condition. Also in this case, an increase of interconnectivity between SFs+intermetallics is found going from $60.7 \pm 7.6 \%$ of the total SFs+intermetallics volume fraction for T6S to $96.6 \pm 0.5 \%$ after creep (GP). This shows that a morphological modification takes place not only for the Si phase but also for the intermetallics and this change affects also the interconnectivity of the

hybrid structure. Finally, the composite in T6S condition shows a connectivity of $95.3 \pm 1.4 \%$ already prior to the creep exposure if all the components building the hybrid structure are analysed (Si+SFs+intermetallics). Even here there is an increase of interconnectivity for the GP condition reaching an almost complete interconnection of $99.2 \pm 0.2 \%$.

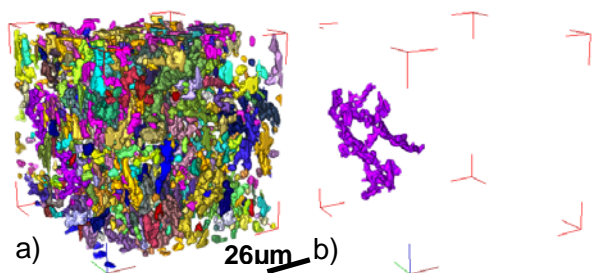


Fig. 8. Reconstructed volume of the T6S condition showing in a) the different Si particles (every particle has a different colour) and in b) the biggest Si particle in the volume of $150 \times 150 \times 150$ voxels ($1.16 \times 10^{-3} \text{ mm}^3$).

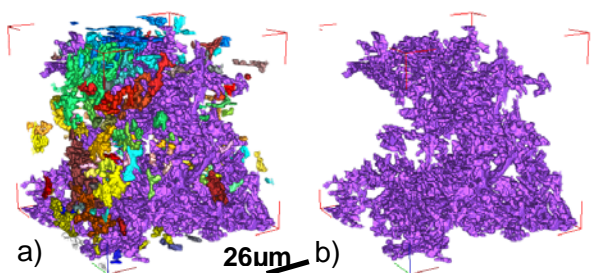


Fig. 9. Reconstructed volume after 6400 h of creep exposure (GP condition) showing in a) the different Si particles (every particle has a different colour) and in b) the biggest Si particle in the volume of $150 \times 150 \times 150$ voxels ($1.16 \times 10^{-3} \text{ mm}^3$).

3.3 Short Fibres Orientation

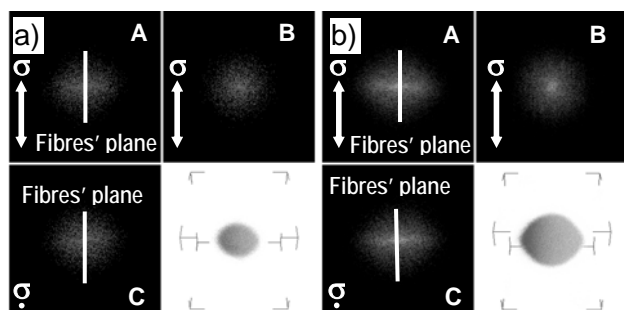


Fig. 10. Results of the 3D FFT obtained using the binarized volumes of the SFs for a) T6S and b) crept GP conditions, respectively. The orientation of the fibres' plane can be recognized in A and C (plane perpendicular to the load direction) for both conditions.

Fig. 10 a) and b) show characteristic results obtained for the 3D FFT investigations for the T6S and GP conditions, respectively. The ellipsoid is cut in three different perpendicular planes passing through the center of the ellipsoid, two of them parallel to the load direction (A and B) and one of them perpendicular to the load direction (C). A and C show a certain degree of orientation both before and after the creep tests. This is due to the random planar orientation of the fibres. The plane parallel to the load direction containing the fibres' plane does not show any preferable orientation of the SFs for both studied conditions. This is in accordance with the fact that the randomly oriented SFs in the T6S condition were not reoriented significantly during 6400 h of creep exposure.

3.4 Creep Damage

Fig. 11 shows two reconstructed volumes of $256 \times 256 \times 256$ voxels for the case of the T6S (a) and GP (b) samples, where only the voids are visible. The difference in void volume fraction can be clearly observed. A quantitative analysis carried out on 8 volumes of the above mentioned size for both studied conditions showed an increase in void volume fraction by a factor 2 after 6400h of creep exposure. However, analysing the amount of voids in reconstructed volumes of the same size, values of $(25 \pm 5) \times 10^{-5}$ and $(26 \pm 5) \times 10^{-5}$ are obtained for the T6S (untested) and GP (after 6400h of creep) samples, respectively.

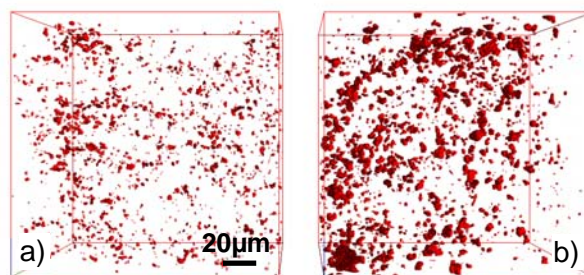


Fig. 11. Reconstructed volumes showing the voids in: a) T6S and b) GP after 6400 h of creep exposure. Size of the volumes: $256 \times 256 \times 256$ voxels ($5.75 \times 10^{-3} \text{ mm}^3$).

The location of the voids was studied qualitatively for the GP condition analysing different volumes and the interactions between the voids and the other phases. Fig. 12 and Fig. 13 show representative reconstructed volumes for which only the voids are shown in a) and the same voids together with the SFs and intermetallics (blue) are shown in b). Fig.12 presents a view along the axis of the creep load, whereas Fig.13 looks perpendicular parallel to the fibre plane containing the load

direction. It is clearly observed that fibre-free-zones as well as intermetallic-free-zones are at the same time pore-free-zones. This means that the pores are

located at interfaces between fibres or between intermetallics.

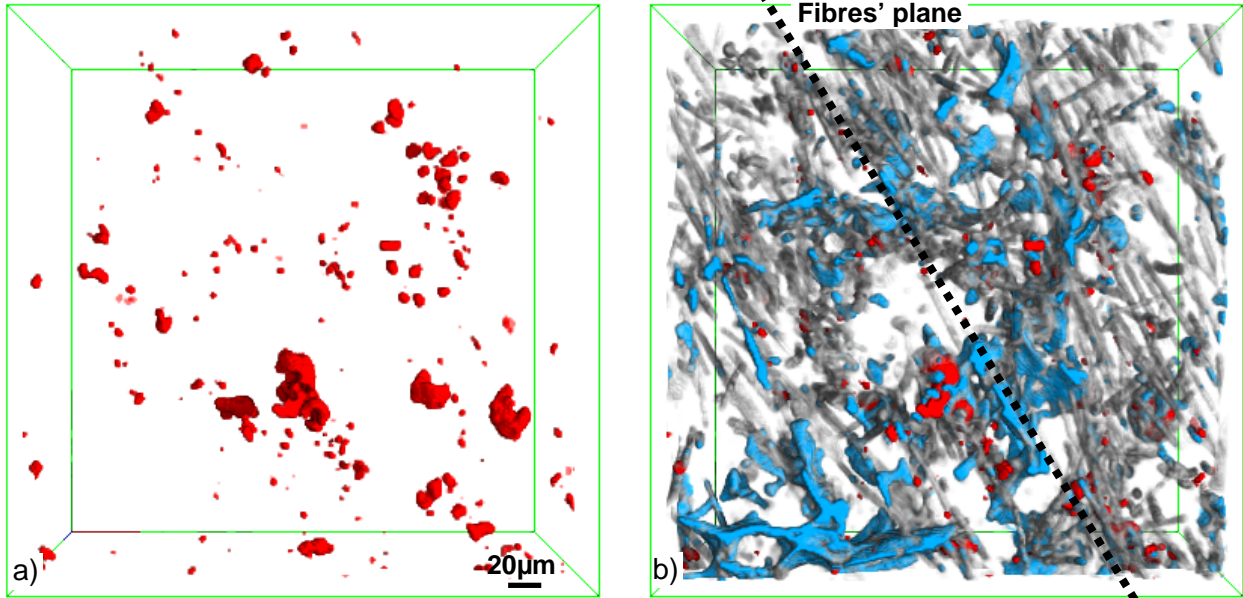


Fig. 12. Reconstructed volume for the GP condition showing in a) the bigger voids and in b) their location with respect to intermetallics and SFs. The load direction is perpendicular to the paper's plane. Size of the volume: 256x256x51 voxels.

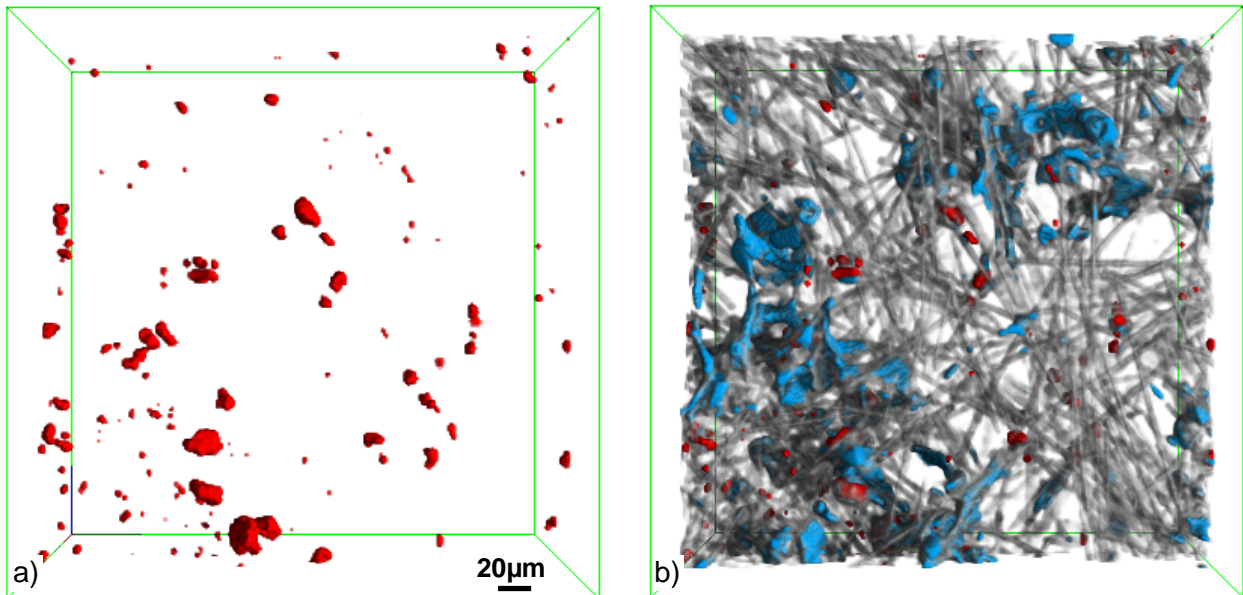


Fig. 13. Reconstructed volume for the GP condition showing in a) the bigger voids and in b) their location with respect to intermetallics and SFs. The vertical axis corresponds to the load direction. Size of the volume: 68x256x256 voxels.

4 Discussion

4.1 Interconnectivity of the Hybrid Structure and Short Fibres Reorientation

The initial hypothesis of a possible change of the interconnectivity of the hybrid reinforcement during long-term creep exposure proposed in [4] has been confirmed and quantified during the present investigations. The diffusion driven Si spheroidisation observed during heat treatments at higher temperatures (and shorter exposure times) in AlSi alloys [5, 21] takes place in the investigated SFRM already at 300°C where the solubility of Si in Al is only 0.1% [20]. This effect could be firstly observed by a 2D analysis, where the coarsening of the Si regions results in an increase of their area by a factor of 2 (see Fig. 6 and Fig. 7). Although this is a relatively straightforward methodology to determine the morphology change of Si during creep exposure, it does not provide information on the real shape and size of the Si particles. The reconstructed volumes obtained from μ CT experiments revealed the real architecture of the constituents of the components as well as the interaction between them. Thus, it was determined that the spheroidisation of Si during long-term creep exposure produces the coalescence of individual Si particles reaching around 70 % of interconnectivity (see Fig. 8 and Fig. 9). The corresponding decrease in the number of particles by a factor of 3 is underestimated since counted particles located at the borders of the studied volumes may also be interconnected outside. On the other hand, the intermetallic particles show an increase of interconnectivity with the short fibres. This suggests a similar diffusion driven coarsening of the intermetallics. Altogether, the changes of the morphology of Si and intermetallics result in a practically full interconnectivity of the hybrid 3D structure. Furthermore, the high degree of interconnectivity of Si after long-term creep exposure (at least 70 %) means that the Si-SF-intermetallics hybrid structure evolves from a SF-intermetallics structure connected by Si bridges (Fig. 14 a) into a SF-intermetallics structure joined by a 3D Si-structure with a high degree of interconnectivity (see Fig. 14 b). The mechanism by which the coarsening of Si and intermetallics provokes this increase of interconnectivity can be understood taking into account that the mean jump frequency of atoms at boundaries or surfaces is much higher than that in the bulk material [22]. Thus, the surface of the SFs represents high diffusivity

paths along which the atoms of eutectic-Si and of the intermetallic phases will preferentially diffuse enhanced by creep resulting in an agglomeration of material at the interfaces of the SFs and a subsequent increase of the interconnectivity of the structure.

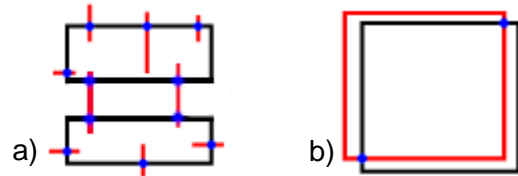


Fig. 14. Schematic representation of the hybrid Si-SF-intermetallics structure: a) SF-intermetallics structure (black rectangles) connected by Si bridges (red lines) and b) SF-intermetallics structure superimposed with an interconnected structure of the Si (red square).

The results obtained using the 3D FFT method did not show any appreciable change of the fibres' orientation during long-term creep. However, the sensitivity of the technique for the investigated set of data requires orientation changes of more than 6°, which is too wide to reveal smaller reorientations of the fibers.

4.2 Creep Damage

The creep tests of the samples for the present study, were stopped during the secondary creep stage at a strain < 1 % (see Fig. 2). It was concluded during the investigations carried out in [4] that fracture of SFs during creep starts at about 1 % strain, where the SFRM enters in tertiary creep. The current μ CT results did not show the presence of fractured SFs in the whole volume of the investigated samples. However, Eggeler [23] showed the presence of broken SFs already in the early stages of creep (0.3 of creep lifetime and about 0.6 % strain) with crack widths < 0.5 μ m. This indicates that the spatial resolution of the μ CT (0.7 μ m) used in this work was too low to detect these cracks. Nevertheless, the increase of porosity during long-term creep before reaching the tertiary creep stage could be detected and quantified using microtomography. The initial porosity volume fraction is increased by a factor 2 during 6400 h of creep exposure. However, no increase was found in the number of voids per volume. Furthermore, investigations of voids' locations showed that these are at interfaces between SFs or intermetallic particles and the matrix with Si. All these considerations lead to the conclusion that the dominating mechanism responsible for the increase of void volume fraction is the diffusional growth of

pores formed during processing of the SFRM and not the creep induced formation of new pores. However, the increase of pore volume fraction during secondary creep is counteracted by the increase of interconnectivity of the hybrid reinforcement so that no detrimental effect for the creep resistance of the SFRM is observed.

5 Conclusions

Synchrotron μ CT was applied for an AlSi12CuMgNi reinforced with 15 vol% of Al₂O₃ SFs before and after 6400 h of creep exposure at 300 °C. The following results were obtained during qualitative and quantitative analysis of the reconstructed volumes:

- Diffusion driven spheroidisation and coalescence of the eutectic-Si takes place during creep exposure. Although a 2D analysis could qualitatively prove the change of shape of Si, the 3D coalescence of individual Si particles is revealed clearly by μ CT.
- The change in morphology of both the eutectic-Si as well as the intermetallic particles result in an increase of interconnectivity of the hybrid Si-SF-intermetallics structure. An almost completely interconnected network is obtained after 6400 h of creep exposure constituted by a SF-intermetallics structure combined with a 3D Si structure which itself exhibits a high degree of connectivity (at least 70 % for the investigated volumes). The high diffusivity paths along the interfaces of the SFs are responsible for the accumulation of Si next to fibres and the subsequent increase of interconnectivity.
- The morphology changes during long-term creep exposure are able to reduce the creep rate by increasing the load carrying capacity of the interconnected hybrid reinforcement [4].
- No significant change in the orientation of the SFs during creep could be determined in the present work. A method with a higher resolution would have to be implemented.
- Although the investigated samples were taken from the secondary creep stage, an increase of voids' volume fraction by a factor of 2 was found. However, a local qualitative analysis of the voids' sites shows that new voids are not generated in addition to the voids originated from the infiltration process, but the latter grow. The negative effects of void growth on the creep resistance of the SFRM are counteracted by the

increase of interconnectivity of the hybrid reinforcement.

Finally, the results obtained in this study provide a new insight on the real architecture of this kind of short fibre reinforced metals which should be considered rather as interpenetrating hybrid composites than as discontinuously reinforced metals. The architecture of such interconnected hybrid reinforcements may change during creep exposure due to enhanced diffusion along the interfaces.

6 Acknowledgements

G. Requena, E. Marks and H. P. Degischer would like to thank the financial support provided by the Austrian Science Fund (project number P19634-N19).

We acknowledge the European Synchrotron Radiation Facility for provision of synchrotron radiation facilities at the ID19 beamline.

References

- [1] <http://mmc-assess.tuwien.ac.at>
- [2] Jiang Z., Lian J., Yang D., Dong S. "An analytical study of the influence of thermal residual stresses on the elastic and yield behaviours of short fiber-reinforced metal matrix composites". *Materials Science and Engineering*, A248, pp 256-278, 1998.
- [3] Dragone T., Nix W. "Geometric factors affecting the internal stress distribution and high temperature creep rate of discontinuous fiber reinforced metals". *Acta metall. mater.*, 38, pp 1941-1953, 1990.
- [4] Requena G., Degischer H. P. "Creep behaviour of unreinforced and short fibre reinforced AlSi12CuMgNi piston alloy". *Materials Science and Engineering*, A 420, pp 265-275, 2006.
- [5] Lasagni F., Lasagni A., Holzappel C., Mücklich F., Degischer H.P. "Three dimensional characterization of unmodified and Sr-modified Al-Si eutectics by FIB and FIB EDX tomography". *Advanced Engineering Materials*, 8, pp 719-723, 2006.
- [6] Klipfel Y. L., He M. Y., McMeeking R. M., Evans A. G., Mehrabian R. "The processing and mechanical behavior of an aluminum matrix composite reinforced with short fibers". *Acta metall. mater.*, Vol. 38, 6, pp 1063-1064, 1990.
- [7] Merkel M., Thomas K.H. "*Taschenbuch der Werkstoffe*". 6th edition, Fachbuchverlag Leipzig, 2003.
- [8] Huang Y. D., Hort N., Dieringa H., Kainer K. U. "Analysis of instantaneous thermal expansion coefficient curve during thermal cycling in short fiber

- reinforced AlSi12CuMgNi composites”. *Composites Science and Technology*, 65, pp 137-147, 2005.
- [9] Saffil ®. *Saffil technical documents*, 2003
- [10] Akbulut H., Durman M., Yilmaz F. “A comparison of properties in as-cast and heat treated short fiber reinforced Al-Si piston alloys”. *Scr.Mat.* , 36, 7, pp 835-840, 1997.
- [11] “Aluminium Taschenbuch“. Aluminium Verlag, pp 583, 1995.
- [12] Salvo L., Cloetens P., Maire E., Zabler S., Blandin J.J., Buffiere J.Y., Ludwig W., Boller E., Bellet D., Josserond C. “X-ray micro-tomography an attractive characterisation technique in materials science”. *Nuclear Instruments and Methods in Physics Research B*, 200, pp 273-286, 2003.
- [13] Baruchel J., Buffiere J.Y., Maire E., Merle P., Peix G. “*X-Ray tomography in materials science*”. 1st edition, Hermes, 2000.
- [14] Baruchel J., Buffiere J. Y., Cloetens P., Di Michiel M., Ferrie, E., Ludwig W., Maire E., Salvo L. “Advances in synchrotron radiation micro-tomography”. *Scripta Mat.*, 55, pp 41-46, 2006.
- [15] <http://rsb.info.nih.gov/ij/>
- [16] <http://www.tgs.com/>
- [17] <http://www.volumegraphics.com/>
- [18] González R., Woods R.”*Digital image processing*”. 2nd edition, Prentice Hall, 2002.
- [19] <http://rsb.info.nih.gov/ij/plugins/ffj.html>
- [20] Smithells C.J. “*Metals Reference Book*”. 6th edition, Butterworths, 1983.
- [21] Ogris E., Wahlen A., Lüchinger H., Uggowitzer P.J. “On the silicon spheroidization in Al-Si alloys”. *J Lig. Met*, 2 ,4, pp 263-269, 2002.
- [22] Shewmon P. “*Diffusion in solids*”. 2nd edition, TMS, 1989.
- [23] Eggeler G. “On the mechanism of Creep in Short Fibre Reinforced Aluminium Alloys”. *Z. Metallkd*, 85, 1, pp 39-46, 1994.